Vacuum 171 (2020) 109048

Contents lists available at ScienceDirect

Vacuum

journal homepage: http://www.elsevier.com/locate/vacuum

Alloy formation at the Fe-on-Nb and Nb-on-Fe interfaces

Judit Balogh [a,*], László Bujdosó [a], Zsolt Endre Horváth [b], Dénes Kaptás [a], László Ferenc Kiss [a], Akio Nakanishi [c], Szilárd Sajti [a], Edit Szilágyi [a]

[a] Wigner Research Centre for Physics, Hungarian Academy of Sciences, H-1525, Budapest 114, P.O.Box 49, Hungary
[b] Centre for Energy Research, Hungarian Academy of Sciences, H-1525, Budapest 114, P.O. Box 49, Hungary
[c] Department of Physics, Shiga University of Medical Science, Shiga, 520-2192, Japan

ARTICLE INFO

Keywords:
Interface alloying
Interface roughness
Mössbauer spectroscopy
X-ray reflectometry
Rutherford backscattering spectrometry

ABSTRACT

Nb/Fe/Nb vacuum evaporated trilayers were studies by X-ray reflectometry, Rutherford backscattering spectrometry and Mössbauer spectroscopy in order to obtain information on the properties of the Fe-on-Nb and Nb-on-Fe interfaces. According to the Mössbauer analysis the interfaces are rather sharp; chemical mixing forms less than 1 nm thick Fe-rich interfaces at both sides of the Fe layer. Comparison to X-ray reflectometry and Rutherford backscattering spectrometry results indicate that interface alloying and geometrical roughness equally contribute to the element distribution across the Fe and Nb layers.

1. Introduction

There is a continuous interest in multilayers of Nb and Fe as it offers a playground to study a variety of interesting phenomena; magnetoresistivity and oscillatory interlayer magnetic coupling [1], the influence of magnetism on superconductivity [2–7], and the effect of hydrogen charging on the magnetic behavior [8,9]. The possibility of applications, like hydrogen sensing [9] or neutron-optical devices [10] has also emerged. Since the Fe–Nb interface plays a decisive role in all the above phenomena it was studied both theoretically by atomistic modeling of the deposition process [11] and experimentally by investigating the layer growth in situ by RHEED and Auger electron spectroscopy [12] or by STM and LEED [13]. The atomistic modeling [11] suggests an asymmetry of the Fe-on-Nb and Nb-on-Fe interfaces, which depends on the substrate temperature. Experimentally, no intermixing was observed at the Nb/Fe(110) interface in case of room temperature (RT) growth [12]. For the Fe/Nb(110) interface three regimes have been identified depending on the thickness of the Fe layer (t_{Fe}) [13]; layer-by-layer growth for the first two monolayers with no evidence of intermixing ($0 < t_{Fe} < 0.4$ nm), formation of a surface alloy ($0.4 < t_{Fe} < 1$ nm), and stabilization of a pure Fe layer ($t_{Fe} > 1$ nm). It was also shown, however, that applying very low growth rates and appropriate buffer layer a sufficient epitaxial quality can be obtained without intermixing of Nb and Fe [13].

The aim of our work is to study the buried interfaces ex situ in vacuum evaporated polycrystalline Nb/Fe/Nb trilayer structures by Mössbauer spectroscopy, which is an effective method to study the alloy formation and short range atomic neighborhood of the Fe atoms. The hyperfine parameters of the absorbing or emitting Mössbauer atom (^{57}Fe in our case) are basically determined by atoms located in its first two coordination shells even in case of metallic systems [14]. This way, in a structurally perfect and chemically sharp layered structure, it is only two monolayers of Fe atoms at the interface which "feel the presence of other kind of atoms". Due to the modified magnetic and electric properties these atoms are considered as interface atoms, even if chemical mixing is not present in these layers. To reveal differences of bottom and top interfaces of the Fe layer the Mössbauer parameters of Nb/Fe/Nb and Ag/Fe/Nb trilayer pairs of equal Fe layer thickness are compared. The Mössbauer parameters of the Fe-on-Nb interface can be well derived from the Ag/Fe/Nb samples, since the Ag-on-Fe interface is chemically very sharp [15], consequently the amount of Fe atoms perturbed by the Ag layer can be well estimated as 2 monolayers, and the Mössbauer parameters of Fe atoms at the Fe–Ag interface are well known from the literature [16]. It is worth noting, that although Fe and Ag are non-mixing elements, a small intermixing may take place at the Fe-on-Ag interface due to the small surface energy of Ag and the consequent tendency of the Ag atoms to cover the Fe atoms entering the surface during deposition [17]. The Ag-on-Fe interface was found to be more perfect, both structurally and chemically, in different studies [18,19] and that way is more appropriate for our purposes. The Mössbauer parameters of the Nb-on-Fe interface can be derived from the comparison of the Nb/Fe/Nb and Ag/Fe/Nb sample pairs of equal Fe layer

* Corresponding author.
E-mail address: balogh.judit@wigner.mta.hu (J. Balogh).

https://doi.org/10.1016/j.vacuum.2019.109048
Received 22 July 2019; Received in revised form 17 October 2019; Accepted 28 October 2019
Available online 31 October 2019

thickness, as the fitted parameters and the intensity of the different components are compared. For example, if the bottom and top interfaces of the Fe layer are similar, then the hyperfine parameters of the Fe–Nb interface components remain unaltered and the intensity of the Nb–Fe interface sub-spectrum is halved when the top Nb layer is replaced by Ag. The above procedure indicated asymmetry for the Fe–B [20], Fe-Al [21], and Fe–Ti [22], interfaces. In the present case the Mössbauer measurements are complemented by X-ray reflectometry (XRR) and Rutherford backscattering spectrometry (RBS) measurements.

2. Materials and methods

The metallic layers were prepared by vacuum evaporation in a high vacuum chamber with base pressure of 10^{-7} Pa and under $3*10^{-6}$ Pa during evaporation. To avoid significant carbon content of the residual gases a zeolite trap is inserted before the inlet of the turbo pump. The substrates were Si(111) wafers with thin native SiO_2 layer, not removed from the substrate, as it will be seen in the experimental results of RBS and XRR. Ag and Nb were evaporated from Cu cold crucibles by electron guns, and the iron (95% enriched in the ^{57}Fe isotope) was evaporated from a heated W boat. The nominal layer thickness was calculated from the bulk densities and the mass measured by a quartz oscillator during evaporation. Four sample pairs with x = 1.5, 2.5, 3.5, 4.5 nm and the following layer sequences were prepared:

A: 20 nm Nb / x nm ^{57}Fe / 20 nm Nb / Si(111)

B: 10 nm Nb / 20 nm Ag / x nm ^{57}Fe / 20 nm Nb / Si(111)

Additionally, a single sample; 20 nm Nb/1 nm ^{57}Fe/20 nm Nb/Si (111) was also prepared. The ^{57}Fe layers of samples A and B were deposited simultaneously from the W boat placed at equal distances from two identical substrates of 2″ diameter to ensure the equal width of the ^{57}Fe layers of the sample pairs. Similarly, the bottom Nb layers of the sample pairs were deposited simultaneously, but the distance to the substrates was somewhat different, which may result in a small (below 1 nm) difference in the Nb layer thicknesses within the pair. The Nb layers covering the Ag layers in the B samples serve to minimize ex-situ oxidation of the ^{57}Fe layers, since thin Ag layers can be easily fractured during temperature change. The evaporation rates were around 0.2 nm/s for Nb and Ag and 0.05 nm/s for ^{57}Fe. The evaporation rates and the overall layer thickness resulted in sample preparation time in the 11–13 and 17–21 min ranges for A and B samples, respectively. Accordingly, the in-situ oxygen and carbon contamination can be estimated as being under 5 at% due to the around 1 min time necessary for monolayer formation of the residual gases under our vacuum conditions [23]. Further on, lower than 1 at% value of the oxygen contamination can be deduced from susceptibility measurements of 40 nm Nb layer prepared under similar conditions as described above. The appearance of a large diamagnetic signal indicated 8.5 ± 0.1 K superconducting temperature, which taking into account the 9.3 K bulk transition temperature and the sensitivity of 0.9 K/at% for oxygen impurities [24] guarantees the lower than 1 at% oxygen content. The estimated oxygen content is even lower (around 0.5 at%) if the thickness dependence of the transition [25] is taken into account. Hereafter the A and B samples will be denoted as Nb/x Fe/Nb and Ag/x Fe/Nb, respectively, where x gives the thickness of the ^{57}Fe layer in nm units.

The structure of the Nb/4.5 Fe/Nb sample was characterized by XRR and RBS measurements. The XRR measurement was performed by a Bruker AXS D8 Discover diffractometer equipped with Göbel-mirror and a scintillation detector using Cu Kα radiation. The collected reflectivity data were evaluated by using the FitSuite code [26], a free multipurpose software. FitSuite uses a transfer matrix method described in Ref. [27] for calculation of X-ray reflectograms. It treats the interface roughness assuming a Gaussian height distribution and a corresponding error function-type interface depth profile characterized by the standard deviation of the Gaussian, the (rms) roughness, σ. The Gaussian's full width at half maximum FWHM = $2\cdot\sqrt{2\cdot ln2}\cdot\sigma \approx 2.355\cdot\sigma$ covers the central region of the error function profile between 4.8% and 95.2%., as described in Refs. [28,29], and therefore will be referred to as $W_{5\text{-}95}$ interface width.

The RBS measurements were performed using 2000 keV $^4He^+$ ion beam obtained from a 5 MeV Van de Graaff accelerator. The beam was collimated to the necessary dimensions of 0.5 × 0.5 mm^2 with 2 sets of four-sector slits and the measurements were performed with an ORTEC detector with a solid angle of 4.729 msr. The dose of the measurements was 4 μC. The ion current of typically 10 nA was measured by a transmission Faraday cup [30]. To reduce the surface contamination, liquid N_2 trap was used; the vacuum was about 1.5×10^{-4} Pa during the experiments. The RBS spectra were simulated by the RBX code [31].

The magnetic behavior of a Nb/1.0 Fe/Nb sample was studied using a Quantum Design MPMS-5S superconducting quantum interference device (SQUID) magnetometer. The temperature dependence of the magnetization was measured at a constant low magnetic field ($H = 10$ Oe) by means of two protocols. In the ZFC (zero-field cooling) protocol, the sample was cooled from 300 to 5 K at zero field and the magnetization was detected during heating at a constant field. In the FC (field cooling) protocol, the sample is cooled from 300 to 5 K at the same field at which the magnetization is measured during heating. (Apparent "negative" magnetization appears in the ZFC curve of superparamagnetic (SPM) particle systems [32] due to a small (below 1 Oe) remnant field of the equipment.)

Mössbauer spectroscopy measurements were carried out by a conventional constant acceleration spectrometer. To attain the best signal to noise ratio conversion electron Mössbauer spectroscopy (CEMS) was applied and iron enriched in the ^{57}Fe Mössbauer resonant isotope was used for the sample preparation. For the detection of the conversion electrons low background gas filled proportional counter was used with H_2 at low temperatures [33], and 96%He–4%CH_4 gas mixture at room temperature. The spectra were measured by a 50 mCi ^{57}Co(Rh) single line Mössbauer source. The hyperfine field (HF) distributions were evaluated according to the Hesse-Rübartsch method [34], by fitting the amplitudes of a number of sextets with HFs increasing with equal step values. The isomer shift (IS) values are given relative to that of α-Fe at room temperature.

3. Experimental results

Figs. 1 and 2 show XRR and RBS data taken on the Nb/4.5 Fe/Nb sample. To eliminate the mass – depth ambiguity of RBS, i.e., the energy of the scattered particle is a function both of the mass of the target nucleus, and of the depth of the target nucleus in the sample, the RBS measurements were done with two different tilt angles, 7° and 60°, at a scattering angle of 165° as shown in Fig. 2. The energy of the backscattered helium from the surface atoms of any element does not vary with the incident angle of the beam, while signals originating from below the surface will appear to move as the measurement geometry changes. To evaluate the layer composition of a sample it is necessary to interpret all spectra taken on the same spot but at different tilt angles with the same layer structure. The simulated curves of Figs. 1 and 2 were successively evaluated by Fitsuite [26] and RBX code [31], thereby iterating to the common layer description shown in the inset of Fig. 1. This way interpretation of the data combines the sensitivity of XRR to thicknesses and the sensitivity of RBS to element distributions. The fitted parameters of XRR including the refractive indices are given in Table 1. The layer thicknesses were found to be 22.07 nm, 4.75 nm, 19.94 nm and 3.75 nm for the bottom Nb, Fe, top Nb, and Nb_2O_5 layers, respectively. The roughness is only slightly different at the two Fe–Nb interfaces, as being 0.94 nm at the bottom of the Fe layer, i.e. at the Fe-on-Nb interface and 0.78 nm at the top of the Fe layer, i.e. at the Nb-on-Fe interface. Accordingly, the $W_{5\text{-}95}$ interface width is 2.2 nm for the Fe-on-Nb and 1.8 nm for the Nb-on-Fe interface. The difference of

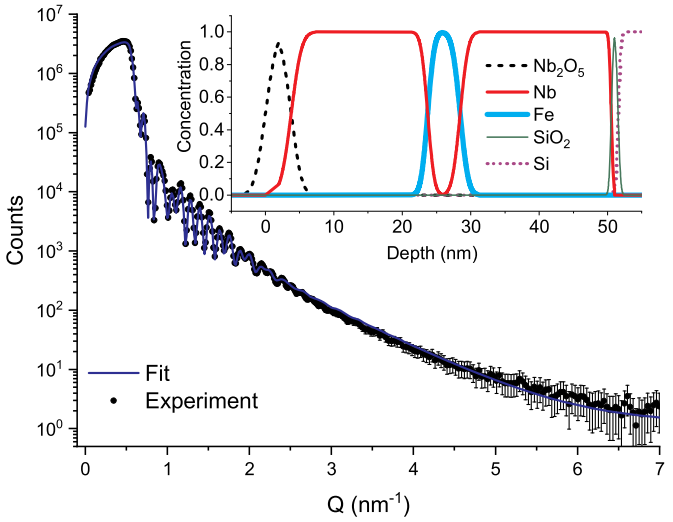

Fig. 1. X-ray reflectivity curve and the concentration profiles. (Color online) Measured (black dots) and fitted (blue line) X-ray reflectivity curve for the 20 nm Nb/4.5 nm ^{57}Fe/20 nm Nb/Si(111) sample. The inset shows the concentration profiles of the different materials corresponding to the fitted parameters. Red (dark) and blue (light) thick lines indicate Nb and Fe, respectively. The components appearing around 0 and 50 nm depth and above - indicated by thin black, green and lilac lines - belong to Nb_2O_5, SiO_2, and Si, respectively. (For interpretation of the references to colour in this figure legend, the reader is referred to the Web version of this article.)

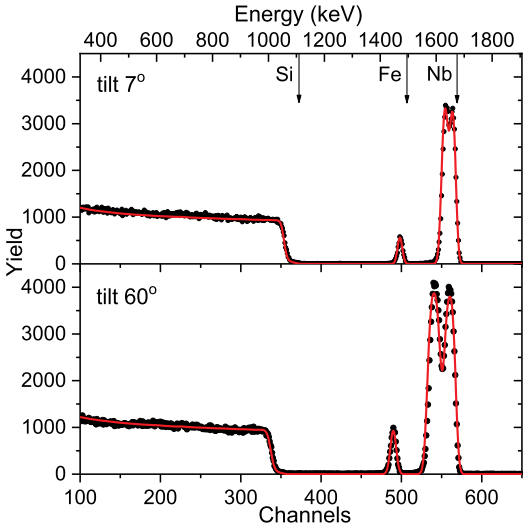

Fig. 2. Rutherford backscattering spectra. (Color online) RBS spectra (black dots) taken on the 20 nm Nb/4.5 nm ^{57}Fe/20 nm Nb/Si(111) trilayer with 2 MeV $^4He^+$ ions for $\Theta = 165°$ scattering angle at tilt 7° and 60°, as indicated in the figure. The energy scale of the backscattered ions is shown on the top. The simulated curve (red line) was evaluated according to the concentration profile shown in Fig. 1. The arrows indicate the energy of helium particles scattered from surface atoms of the corresponding elements. (For interpretation of the references to colour in this figure legend, the reader is referred to the Web version of this article.)

the roughness parameters lies within the overall experimental errors. The overall uncertainty of the layer thickness and the interface roughness are below ±5% and ±20%, respectively, as estimated from measurements at different sample pieces and applying different layer models.

The uncertainty of RBS depends mainly on the statistics and the signal/background ratios [36]. The latter is different for the various

Table 1
The parameters obtained from the fit of x-ray reflectivity measurements. The roughness values refer to the top interface of the respective layer. The complex refractive indices ($n = 1 - \delta + i\beta$), see Ref. [35], were kept constant in the fit. The densities of the Nb_2O_5 and SiO_2 were assumed to be 4.6 and 2.2 g cm^{-3}, respectively. Based on various model simulations we estimate the overall uncertainty of the layer thickness and the interface roughness below ±5% and ±20%, respectively.

	Nb_2O_5	top Nb	^{57}Fe	bottom Nb	SiO_2
$\delta \cdot 10^6$	13.56	24.23	22.45	24.23	7.12
$\beta \cdot 10^6$	0.58	1.49	2.90	1.49	0.09
Thickness (nm)	3.75	19.94	4.75	22.07	1
Roughness (nm)	1.27	1.36	0.78	0.94	0.26

elements, typically about 2% for Fe and Nb and much higher (about 20%) for oxygen. However, while on one hand the supplementation of the layer model with oxygen within the Fe or the Nb layer was not imperious, therefore significant amount of oxygen can be excluded in these layers, on the other hand the thin layers of SiO_2 with a thickness of 1 nm over the Si substrate and Nb_2O_5 over the top Nb layers, improved the agreement between the measured and simulated curves at the Si/Nb interface and at the Nb surface. It is important to note that these oxide layers are probably formed ex-situ, not in the deposition chamber.

The room temperature CEMS spectra of the four as-received sample pairs are shown in Fig. 3a. All spectra were fitted by a set of sextets with hyperfine fields allowed in the 5–35T range and a broadened doublet with a single quadrupole splitting (QS). The evaluated normalized HF distributions are shown in Fig. 3b and for better visibility the 5–30 T range is enlarged for the 2.5, 3.5 nm and 4.5 nm iron thickness samples. The Nb/1.0 Fe/Nb sample and two sample pairs (1.5 nm and 2.5 nm Fe layer thicknesses) have also been measured at 20 K. The low temperature spectra of the latter two sample pairs and the fitted HF distributions are shown in Fig. 4a and b, respectively, while the RT and 20 K spectra of the Nb/1.0 Fe/Nb sample is shown in Fig. 5a. In the spectrum fittings the line-width of the sextet components of the HF distribution was fixed to the experimental line-width (0.24 mm/s) of the spectrometer, the HF step value was an iteration parameter in the 0.71–0.72T range, the isomer shift (IS) was assumed proportional to the HF, and no QS was allowed. The intensities of the second and fifth lines relative to that of line three and four of the sextets were close to 4 in each case, indicating an in-plane orientation of the Fe magnetic moments.

The most important parameters of the Mössbauer spectra are summarized in Table 2 and Table 3. The magnetic component is divided into two subgroups for each spectrum. The one indicated as bcc-Fe, is a sum of the sextets in the 29.3 T–33 T range at RT and accordingly in the 30.1 T −33.8 T range at 20 K. The sum of the sextets in the 5 T–29.3 T range at RT and 5 T −30.1 T range at 20 K is indicated as magnetic alloy. In thin layers the local dipole fields and finite size effects may slightly reduce the hyperfine field of the Fe atoms and this variation cannot be distinguished from that resulting from the presence of impurity atoms in the local neighborhood. The field ranges were fixed according to the literature results on dilute alloys of Nb in α-Fe with the Nb concentration up to about 5 at.% by Ref. [37] and according to observations on the local dipole fields in thin layers [15]. This assignment allows a less than 3 at% Nb content of the bcc-Fe layer, but takes into account the possible effect of local dipole fields. It is also worth noting, that the evaluated distributions show close to zero probabilities around the 30 T field value for the 3.5 nm and 4.5 nm Fe samples. The spectral fraction of the different components (bcc-Fe, paramagnetic alloy, magnetic alloy) was transformed into Fe equivalent layer thicknesses by multiplying the respective fraction with the nominal thickness of the Fe layer. (The Mössbauer-Lamb factors were assumed equal for all components.) The Fe equivalent layer thicknesses are labeled as d_{bcc}, d_{para}, and d_{mag} for the bcc-Fe, for the paramagnetic alloy and for the magnetic alloy components, respectively. The amount of iron at the interface in Fe equivalent layer thickness is given as; $d_i = d_{para} + d_{mag}$.

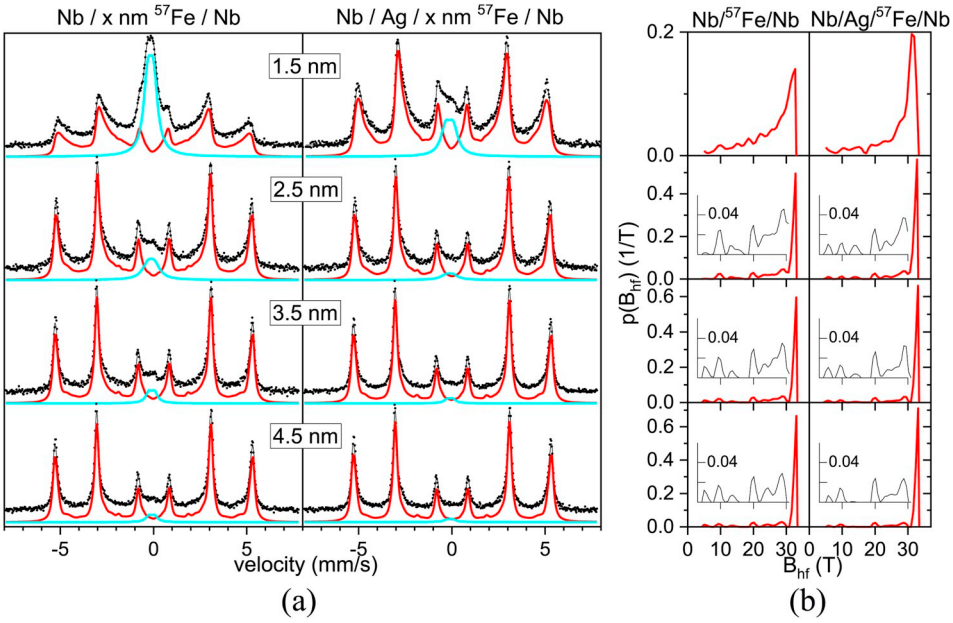

Fig. 3. Mössbauer spectra and hyperfine field distributions at RT. (Color online) Mössbauer spectra of the as received samples measured at RT (a) and the evaluated HF distributions (b). The sub-spectra belonging to the fitted doublet component and to the HF distribution are indicated by blue (light) and red (dark) lines, respectively, while the sum of the two components is shown by black lines. In (b) the horizontal (HF) scales are the same for all HF distributions, while the vertical intensity scales are normalized to unit area and vary from graph to graph. Where necessary for the visibility, the vertical scale is enlarged in the inset. (For interpretation of the references to colour in this figure legend, the reader is referred to the Web version of this article.)

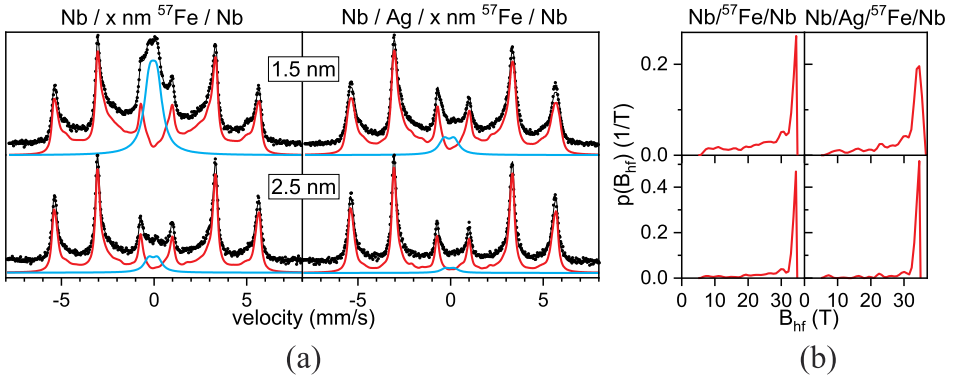

Fig. 4. Mössbauer spectra and hyperfine field distributions at 20 K. (Color online) Mössbauer spectra of the indicated samples at 20 K (a) and the evaluated HF distributions (b). The sub-spectra belonging to the fitted doublet component and to the HF distribution are indicated by blue (light) and red (dark) lines, respectively, while the sum of the two components is shown by black lines. In (b) the horizontal (HF) scales are the same for all HF distributions, while the vertical intensity scales are normalized to unit area and vary from graph to graph. (For interpretation of the references to colour in this figure legend, the reader is referred to the Web version of this article.)

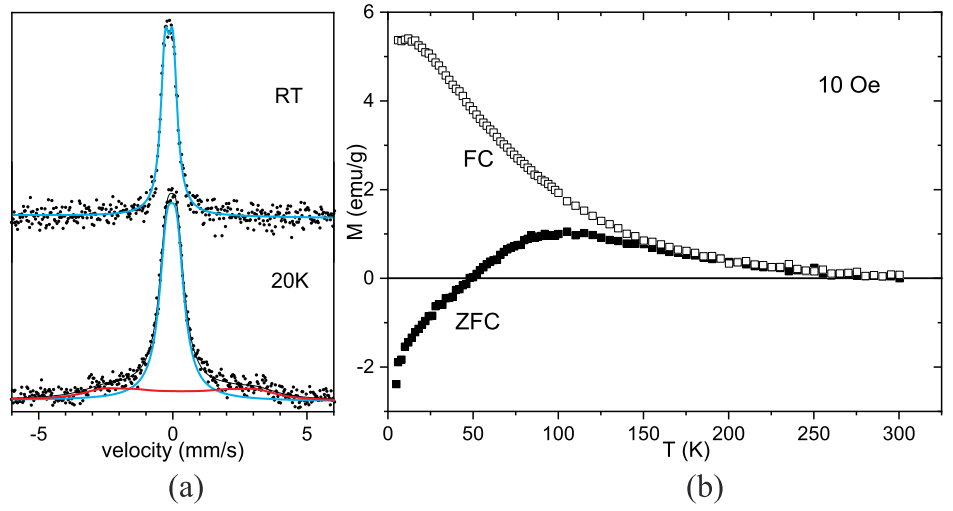

Fig. 5. Mössbauer spectra and temperature dependence of the magnetization for the Nb/1.0 Fe/Nb sample (Color online) Mössbauer spectra of the 20 nm Nb/1 nm ^{57}Fe/20 nm Nb sample measured at RT and 20 K. The paramagnetic and the magnetic subspectra are indicated by blue (light) and red (dark) lines, respectively (a). Temperature dependence of the magnetization measured by SQUID according to the FC-ZFC protocol, as described in the text (b). (For interpretation of the references to colour in this figure legend, the reader is referred to the Web version of this article.)

The RT and 20 K Mössbauer spectra of a Nb/1.0 Fe/Nb sample is shown in Fig. 5, together with the FC-ZFC magnetization of the sample measured by SQUID. Both the RT and the 20 K spectra shows a quadruple doublet with parameters (IS = −0.142 (−0.042) mm/s and QS = 0.292 (0.377) mm/s at RT (20 K)) similar to those of the paramagnetic component of the Nb/1.5 Fe/Nb sample. However, at 20 K the linewidth increases and there appears a broad magnetic component with an about 17 T average hyperfine field, which gives about 30% of the spectral area. This behavior is in line with the FC-ZFC magnetization of the sample in Fig. 5b, which shows a superparamagnetic type behavior with blocking temperature around 100 K.

4. Discussion

From the XRR and RBS results the thicknesses of the Fe (and Nb) layers are slightly larger than the nominal thicknesses; the thickness of the ^{57}Fe layer is 4.75 nm instead of the 4.5 nm nominal value. The Fe-on-Nb and Nb-on-Fe interfaces are characterized by the roughness of the bottom Nb and the ^{57}Fe layers, respectively, in case of the XRR measurement, however, specular reflectivity does not distinguish the interface roughness and the laterally homogeneous intermixing e.g. due to inter-diffusion. One has to note that in the RBS simulation supposing atomically sharp interfaces provide similar (or better) χ^2 values, i.e. the $W_{5\text{-}95}\sim$2 nm wide interface layers are not resolved well by RBS. It is also worth mentioning that the surface area measured by RBS is much smaller than the one contributing to XRR, i.e. the geometrical component of the interface roughness may be different.

The most direct experimental information on the range of the chemical mixing is expected to be gained from Mössbauer spectroscopy, since the hyperfine parameters are mainly determined by the atoms sitting in the first two coordination shells of the resonant ^{57}Fe atom and geometrical interface roughness with several nm lateral scales makes small perturbation of these coordination shells.

The RT Mössbauer spectra of the studied samples consist of a paramagnetic and a magnetic component with varying ratio, as can be seen in Fig. 3. For large enough thickness of the deposited Fe the formation of a bcc-Fe layer and two separated interfaces, Fe-on-Nb and Nb-on-Fe, are expected. The formation of two well separated interfaces is signaled by constant values of the HF parameters and of the interface width as a function of the deposited Fe thickness. Indeed, the spectral contribution of the Fe–Nb interface component, $d_i^{Nb/Fe/Nb} = d_{para} + d_{mag,}$ decreases gradually with increasing thickness of the deposited Fe layer, but its value stays around 1 nm for the Nb/2.5 Fe/Nb, Nb/3.5 Fe/Nb and Nb/4.5 Fe/Nb samples. Similarly, the interface component of the Ag/Fe/Nb samples, $d_i^{Ag/Fe/Nb}$, saturates at around 0.7 nm, but in this case d_{mag} contains contribution of the Ag-on-Fe interface which makes about two monolayers (~0.3 nm) Fe [15]. Therefore the width of the single Fe-on-Nb interface, $d_i^{Fe\text{-}on\text{-}Nb} = d_i^{Ag/Fe/Nb}$-0.3 nm, is around 0.4 nm and evidently $d_i^{Nb\text{-}on\text{-}Fe} = d_i^{Nb/Fe/Nb}$ - $d_i^{Fe\text{-}on\text{-}Nb}$ ~0.6 nm. Here it has to be emphasized that these values are averages of the local interface widths experienced by the resonant ^{57}Fe atoms over the sample area. Taking into account an estimated 10–20% error of the calculated values, one can say that both interfaces are rather sharp and the small difference lies within the experimental errors.

Further verification of the interface thickness is given by measurement of the Nb/1.0Fe/Nb sample. The 1 nm overall interface thickness in the Nb/Fe/Nb samples means, that no bcc-Fe layer is formed when the thickness of the deposited Fe layer is equal to or below this value. This indeed seems to be the case. Even though the Nb/1.5Fe/Nb sample contains components attributed to bcc-Fe (see Table 2 and Table 3) the Nb/1.0Fe/Nb sample is fully paramagnetic at RT, as can be seen from both the SQUID magnetization curve and the Mössbauer spectrum of Fig. 5. Since the amount of the magnetic interface components surpasses the paramagnetic ones both at RT and 20 K for all the other samples (see Table 3), the lack of magnetic alloy component at RT in the Nb/1.0Fe/Nb sample may seem surprising. The explanation lies in the superparamagnetic behavior of the magnetic components, as shown in the SQUID measurement by the deviation of the FC and ZFC magnetization curves measured in 10 Oe. Accordingly, the Mössbauer spectrum also exhibits magnetic components at 20 K, as shown in Fig. 5a. The superparamagnetic behavior of ultrathin magnetic layers is commonly attributed to the discontinuities of such layers. Superparamagnetic regions are probably also present in the Ag/1.5 Fe/Nb and Nb/1.5 Fe/Nb samples and contribute to the slightly increased values of d_{para} both at RT and 20 K. Above 2.5 nm deposited Fe thickness the paramagnetic component remains constant within the experimental errors at RT indicating that the magnetic layers are continuous or magnetically coupled. Since at 20 K the increased hyperfine field of the Ag–Fe interface [15] may perturb the ratio of d_{bcc} and d_{mag} the rest of the samples were not measured at 20K and the interface widths was calculated from the RT spectral fractions.

The determination of the alloy phases formed at the interfaces is not easy, since the interfaces are rather sharp. The nonmagnetic components of the RT spectra may indicate the presence of several crystalline and amorphous alloy phases; crystalline Fe_2Nb, FeNb, solid solution of Fe in Nb [37–40], and amorphous $Fe_xNb_{100\text{-}x}$ alloys in the $20 < x < 80$ concentration range [41–43]. The observed IS and QS values suggest an amorphous phase, but the presence of some crystalline phases around the Fe_2Nb and FeNb concentrations cannot be fully excluded. The component labeled as magnetic alloy should also belong to Fe atoms in the interface region. The magnetic alloy of the interface has a broad distribution with an average hyperfine field in the 20T −23 T range both at RT and 20 K. While the peak close to 29 T can be due to Fe atoms with one Nb atom in the first coordination shell, the peaks around 10 T and 20 T hyperfine fields are more difficult to correlate with local atomic arrangements, since such components are not observed in bulk alloys [38,40]. The low hyperfine field values certainly indicate non-equilibrium Nb-rich environments, as they can be found in Fe–Nb multilayers [44] and mechanically alloyed samples [45,46], but the small spectral fraction and the broad hyperfine field range results in a

Table 2
Mössbauer parameters of the spectra measured at RT and 20 K; Isomer shift (IS), quadrupole splitting (QS) and linewidth (W) of the doublet, average hyperfine field of the bcc Fe (HF_{bcc}) and the magnetic alloy component (HF_{mag}). The errors shown are the statistical errors and f denotes that the parameter is fixed.

	IS (mm/s)	QS (mm/s)	W (mm/s)	HF_{bcc} Tesla	HF_{mag} Tesla
T = RT					
Ag/1.5 Fe/Nb	−0.131(6)	0.403(14)	0.608 (49)	31.26(7)	21.63(7)
Nb/1.5Fe/Nb	−0.155(2)	0.311(4)	0.524 (13)	31.49(7)	21.45(7)
Ag/2.5 Fe/Nb	−0.125(f)	0.361(f)	0.698(f)	32.28(14)	21.86(14)
Nb/2.5 Fe/Nb	−0.125 (11)	0.361(36)	0.698 (99)	32.28(12)	21.77(12)
Ag/3.5 Fe/Nb	−0.096(f)	0.302(f)	0.415(f)	32.60(12)	20.12(12)
Nb/3.5 Fe/Nb	−0.096 (13)	0.301(25)	0.415 (73)	32.54(12)	20.07(12)
Ag/4.5 Fe/Nb	−0.096(f)	0.302(f)	0.415(f)	32.71(13)	20.78(13)
Nb/4.5 Fe/Nb	−0.096(f)	0.302(f)	0.415(f)	32.65(12)	19.78(12)
T = 20 K					
Ag/1.5 Fe/Nb	−0.086(9)	0.559(20)	0.682 (58)	33.87(7)	21.68(7)
Nb/1.5Fe/Nb	−0.047(3)	0.409(14)	0.716 (30)	33.47(5)	20.92(5)
Ag/2.5 Fe/Nb	−0.048(f)	0.472(f)	0.596(f)	33.85(13)	20.54(13)
Nb/2.5 Fe/Nb	−0.048 (12)	0.472(26)	0.596 (70)	33.75(9)	21.86(9)

Table 3
The amount of iron in Fe equivalent layer thickness as calculated from the spectral intensities and the nominal thickness of the deposited Fe layer in the bcc Fe, in the paramagnetic and in the magnetic alloy components (d_{bcc}, d_{para}, and d_{mag}, respectively), in the full interface ($d_i^{Ag/Fe/Nb}$, $d_i^{Nb/Fe/Nb}$), and the calculated $d_i^{Fe\text{-}on\text{-}Nb}$ and $d_i^{Nb\text{-}on\text{-}Fe}$ values (see the Discussion for explanation).

	d_{bcc} (nm)	d_{para} (nm)	d_{mag} (nm)	$d_i^{Ag/Fe/Nb}$ (nm)	$d_i^{Nb/Fe/Nb}$ (nm)	$d_i^{Fe\text{-}on\text{-}Nb}$ (nm)	$d_i^{Nb-on-Fe}$ (nm)
			T = RT				
Ag/1.5 Fe/Nb	0.70	0.18	0.61	0.79	–	0.49	–
Nb/1.5Fe/Nb	0.39	0.52	0.59	–	1.11	–	0.62
Ag/2.5 Fe/Nb	1.82	0.10	0.58	0.68	–	0.38	–
Nb/2.5 Fe/Nb	1.51	0.25	0.74	–	0.99	–	0.61
Ag/3.5 Fe/Nb	2.83	0.08	0.59	0.67	–	0.37	–
Nb/3.5 Fe/Nb	2.49	0.18	0.84	–	1.02	–	0.65
Ag/4.5 Fe/Nb	3.78	0.07	0.65	0.72	–	0.42	–
Nb/4.5 Fe/Nb	3.46	0.16	0.88	–	1.04	–	0.62
			T = 20 K				
Ag/1.5 Fe/Nb	0.95	0.12	0.43	0.55	–	0.25	–
Nb/1.5Fe/Nb	0.55	0.42	0.53	–	0.95	–	0.70
Ag/2.5 Fe/Nb	2.04	0.08	0.38	0.46	–	0.16	–
Nb/2.5 Fe/Nb	1.62	0.21	0.67	–	0.88	–	0.72

large uncertainty of the evaluated distributions.

In order to relate the results of the Mössbauer measurements to those of XRR and RBS, we attempt to estimate the thicknesses of the interfaces ($D^{Fe\text{-}on\text{-}Nb}$, $D^{Nb\text{-}on\text{-}Fe}$) from the Fe equivalent layer thicknesses ($d_i^{Nb\text{-}on\text{-}Fe}$, $d_i^{Fe\text{-}on\text{-}Nb}$). In lack of experimental data on the density, all thicknesses will be calculated using the bulk densities, the molar masses of the elements (ρ_{Fe}, ρ_{Nb}, M_{Fe}, and M_{Nb}, resp.), and the atomic concentration of Fe in the respective alloy (c_{Fe}) as follows:

$$D = d\left(1 + \frac{\rho_{Fe} M_{Nb}(1 - c_{Fe})}{\rho_{Nb} M_{Fe} c_{Fe}}\right). \quad (1)$$

Precise determination of the alloy concentrations or the concentration distributions is impossible from the present Mössbauer spectra, therefore it will only be estimated based on some considerations. The average Fe content of the interface is probably well above 50 at%, since the IS value of the paramagnetic component suggest an iron rich amorphous phase [41] and according to the large average hyperfine field, the magnetic component should also belong to non-equilibrium regions with Fe concentrations above 66 at%. Supposing $Fe_{70}Nb_{30}$ average alloy concentration of the interface eq. (1) provides $D^{Fe\text{-}on\text{-}Nb} = 0.66$ nm and $D^{Nb\text{-}on\text{-}Fe} = 0.99$ nm. These values are smaller than those obtained from the XRR measurement; 2.2 nm for the Fe-on-Nb and 1.8 nm for the Nb-on-Fe interface and remain significantly smaller even if the calculations are made using the 5% larger experimental thickness of the Fe layer concluded from the XRR and RBS results, rather than the nominal one. The difference suggests that interface alloying and geometrical roughness equally contribute to the element distribution across the rather sharp Fe–Nb interfaces. Asymmetry of the interfaces cannot be approved since the small but opposite asymmetries observed by the different methods lie within the experimental errors.

Comparing our results to those obtained for epitaxially grown substrate layers [12,13] there is an acceptable agreement for the width of the intermixed region in case of the Fe-on-Nb interface. The $d_i^{Fe\text{-}on\text{-}Nb}$ ~0.4 nm value deduced from the Mössbauer results is even smaller than the about 1 nm threshold limit of the deposited Fe thickness given by Mougin et al. [12] for the appearance of pure bcc-Fe over Nb(110). The smaller value may be due to our Mössbauer evaluation which allows a few per cent Nb impurities in the Fe layer. The close values are noticeable since both the substrate material and the growth conditions were very different. The Nb-on-Fe interface is less abrupt ($d_i^{Nb\text{-}on\text{-}Fe}$~ 0.6 nm) in our samples than those observed for Fe(110) substrate layers by Wolf et al. [13], but taking into account the thin polycrystalline Fe substrate layers of our samples in contrast to the thick (10 nm) epitaxially grown Fe islands studied by Wolf et al. [13], the difference is not surprising. Grain boundaries, voids or small disordered regions can certainly enhance the mixing processes. Beyond the thickness of the interface, our Mössbauer spectroscopy results provide information on the alloy composition of the interface, as well, which can influence e.g. the superconducting proximity effect. The non-monotonic variation of the superconducting temperature as a function of the Fe layer thickness in Fe/Nb [2] and Fe/Nb/Fe [7] layer structures was explained by supposing a non-magnetic alloy component at the interfaces. Our observation of the paramagnetic fraction at both the Nb-on-Fe and the Fe-on-Nb interfaces proves the multiphase nature of both interfaces.

In summary we can say that chemically rather sharp and symmetric interfaces can be achieved in polycrystalline Nb/Fe/Nb trilayers, which may be appropriate for studying the different application possibilities.

5. Conclusion

The buried interfaces of Nb/Fe/Nb vacuum evaporated trilayers on top of Si(111) substrate were studied by X-ray reflectometry, Rutherford backscattering spectrometry and Mössbauer spectroscopy in order to obtain information on the properties of the Fe-on-Nb and Nb-on-Fe interfaces. According to the Mössbauer analysis the chemical mixing forms less than 1 nm thick Fe-rich interfaces at both sides of the Fe layer, while evaluation of the XRR and RBS measurements provide $W_{5\text{-}95} \sim 2$ nm wide interface layers indicating that chemical mixing and geometrical roughness equally contribute to the element distribution across the layers. Both interfaces are multiphase with Fe rich average composition. The results show that chemically rather sharp and symmetric interfaces can be obtained in polycrystalline Nb/Fe/Nb trilayers over commercial Si substrates.

Acknowledgement

The authors acknowledge financial support of the Hungarian Scientific Research Fund (OTKA) [grant K112811].

References

[1] J.E. Mattson, C.H. Sowers, A. Berger, S.D. Bader, Magnetoresistivity and oscillatory interlayer magnetic coupling of sputtered Fe/Nb superlattices, Phys. Rev. Lett. 68 (1992) 3252, https://doi.org/10.1103/PhysRevLett.68.3252.
[2] Th Mühge, K. Theis-Bröhl, K. Westerholt, H. Zabel, N.N. Garif'yanov, Y.U. V. Goryunov, I.A. Garifullin, G.G. Khaliullin, Influence of magnetism on superconductivity in epitaxial Fe/Nb bilayer systems, Phys. Rev. B 57 (1998) 5071, https://doi.org/10.1103/PhysRevB.57.5071.
[3] G. Verbanck, C.D. Potter, V. Metlushko, R. Schad, V.V. Moshchalkov, Y. Bruynseraede, Coupling phenomena in superconducting Nb/Fe multilayers, Phys. Rev. B 57 (1998) 6029, https://doi.org/10.1103/PhysRevB.57.6029.
[4] Hiroki Yamazaki, Nic Shannon, Hidenori Takagi, Interplay between superconductivity and ferromagnetism in epitaxial Nb(110)/Au(111)/Fe(110) trilayers, Phys. Rev. B 73 (2006), 094507, https://doi.org/10.1103/PhysRevB.73.094507.

[5] J.M.E. Geers, M.B.S. Hesselberth, J. Aarts, A.A. Golubov, Depairing currents in the superconductor/ferromagnet proximity system Nb/Fe, Phys. Rev. B 64 (2001), 094506, https://doi.org/10.1103/PhysRevB.64.094506.

[6] R. Steiner, P. Ziemann, Magnetic switching of the superconducting transition temperature in layered ferromagnetic/superconducting hybrids: spin switch versus stray field effects, Phys. Rev. B 74 (2006), 094504, https://doi.org/10.1103/PhysRevB.74.094504.

[7] Th Mühge, K. Westerholt, H. Zabel, N.N. Garif'yanov, Y.U.V. Goryunov, I. A. Garifullin, G.G. Khaliullin, Magnetism and superconductivity of Fe/Nb/Fe trilayers, Phys. Rev. B 55 (1997) 8945, https://doi.org/10.1103/PhysRevB.55.8945.

[8] F. Klose, C.H. Rehm, D. Nagengast, H. Maletta, A. Weidinger, Continuous and reversible change of the magnetic coupling in an Fe/Nb multilayer induced by hydrogen charging, Phys. Rev. Lett. 78 (1997) 1150, https://doi.org/10.1103/PhysRevLett.78.1150.

[9] S.J. Callori, C. Rehm, G.L. Causer, M. Kostylev, F. Klose, Hydrogen absorption in metal thin films and heterostructures investigated in situ with neutron and X-ray scattering, Metals 6 (2016) 125, https://doi.org/10.3390/met6060125.

[10] Kyaw Zaw Lin, V.G. Syromyarnikov, Multilayer neutron monochromator-polarizer based on iron, J. Surf. Invest. 10 (2016) 687, https://doi.org/10.1134/S1027451016040121.

[11] A. Canzián, H.O. Mosca, G. Bozzolo, Atomistic modeling comparison of Fe growth on Nb(1 1 0) and Nb growth on Fe(1 1 0), Surf. Sci. 574 (2005) 287, https://doi.org/10.1016/j.susc.2004.10.040.

[12] A. Mougin, S. Andrieu, C. Dufour, K. Dumesnil, Epitaxial growth of Fe on Nb(110), Surf. Sci. 518 (2002) 175, https://doi.org/10.1016/S0039-6028(02)02084-8.

[13] C. Wolf, U. Köhler, Growth and intermixing of Nb on Fe(110) and Fe on Nb(110), Thin Solid Films 500 (2006) 347, https://doi.org/10.1016/j.tsf.2005.11.039.

[14] I. Vincze, I.A. Campbell, Mössbauer measurements in iron based alloys with transition metals, J. Phys. F Met. Phys. 3 (1973) 647, https://doi.org/10.1088/0305-4608/3/3/023.

[15] G. Lugert, G. Bayreuther, Temperature dependence of the hyperfine field and magnetization in ultrathin epitaxial Fe films, Phys. Rev. B 38 (1988) 11068, https://doi.org/10.1103/PhysRevB.38.11068.

[16] J. Balogh, D. Kaptás, T. Kemény, L.F. Kiss, T. Pusztai, I. Vincze, Atomic and magnetic structure of the interface in multilayers, Hyperfine Interact. 141/142 (2002) 13, https://doi.org/10.1023/A:1021206120466.

[17] D.E. Bürgler, C.M. Schmidt, D.M. Schaller, F. Meisinger, R. Hofer, H.J. Güntherodt, Optimized epitaxial growth of Fe on Ag(001), Phys. Rev. B 56 (1997) 4149, https://doi.org/10.1103/PhysRevB.56.4149.

[18] P.J. Schurer, Z. Celinski, B. Heinrich, Mössbauer Investigation of the growth of the Fe multilayer in Fe(100)/Ag(100) structures, Phys. Rev. B 5 (1995) 2506, https://doi.org/10.1103/PhysRevB.51.2506.

[19] G. Sharma, R. Gupta, D. Kumar, A. Gupta, Anomalous evolution of interfaces in Fe/Ag magnetic multilayer, J. Phys. D Appl. Phys. 46 (2013) 505302, https://doi.org/10.1088/0022-3727/46/50/505302.

[20] J. Balogh, L. Bujdosó, D. Kaptás, I. Dézsi, A. Nakanishi, Top and bottom interfaces in Fe-B multilayers investigated by Mössbauer spectroscopy, Phys. Rev. B 85 (2012) 195429, https://doi.org/10.1103/PhysRevB.85.195429.

[21] P. Süle, D. Kaptás, L. Bujdosó, Z.E. Horváth, A. Nakanishi, J. Balogh, Chemical mixing at "Al on Fe" and "Fe on Al" interfaces, J. Appl. Phys. 118 (2015) 135305, https://doi.org/10.1063/1.4932521.

[22] J. Balogh, P. Süle, L. Bujdosó, Z.E. Horváth, D. Kaptás, A. Kovács, D.G. Merkel, A. Nakanishi, S.Z. Sajti, L. Bottyán, Asymmetric alloy formation at the Fe-on-Ti and Ti-on-Fe interfaces, J. Phys. Condens. Matter 30 (2018) 455001, https://doi.org/10.1088/1361-648X/aae508.

[23] A. Roth, Vacuum Technology, Elsevier Science B. V., Amsterdam, The Netherlands, 1976, ISBN 0444108017, p. 2.

[24] DeSorbo Warren, Effect of dissolved gases on superconducting properties of niobium, Phys. Rev. B 132 (1963) 107, https://doi.org/10.1103/PhysRev.132.107.

[25] J. Kodama, M. Itoh, H. Hirai, Superconducting transition temperature versus thickness of Nb film on various substrates, J. Appl. Phys. 54 (1983) 4050.

[26] S.Z. Sajti, L. Deák, L. Bottyán, FitSuite a General Program for Simultaneous Fitting (And Simulation) of Experimental Data, (FitSuite 1.0.5.Rc11), arXiv:0907.2805v1 [cond-mat.other], https://arxiv.org/abs/0907.2805v1.

[27] L. Deák, L. Bottyán, D.L. Nagy, H. Spiering, A common optical algorithm for the evaluation of specular spin polarized neutron and Mössbauer reflectivities, Physica B 297 (2001) 113, https://doi.org/10.1016/S0921-4526(00)00817-6.

[28] R. Röhlsberger, Theory of X-ray grazing incidence reflection in the presence of nuclear resonance excitation, Hyperfine Interact. 123/124 (1999) 301, https://doi.org/10.1023/A:1017063605078.

[29] L. Deák, PhD. Thesis, Roland Eötvös University Budapest, February 1999.

[30] F. Pászti, A. Manuaba, C. Hajdu, A.A. Melo, M.F. da Silva, Current measurement on MeV energy ion beams, Nucl. Instrum. Methods B 47 (1990) 187, https://doi.org/10.1016/0168-583X(90)90028-S.

[31] E. Kótai, Computer methods for analysis and simulation of RBS and ERDA spectra, Nucl. Instrum. Methods B 85 (1994) 588, https://doi.org/10.1016/0168-583X(94)95888-2.

[32] L.F. Kiss, J. Balogh, L. Bujdosó, D. Kaptás, Magnetic properties of Fe-Ag multilayers with varying layer thickness and bilayer number, Phys. Rev. B 98 (2018) 144423, https://doi.org/10.1103/PhysRevB.98.144423.

[33] K. Fukumura, A. Nakanishi, T. Kobayashi, Hydrogen-filled proportional counter operated at low temperatures and its application to CEMS, Nucl. Instrum. Methods B 86 (1994) 387, https://doi.org/10.1016/0168-583X(94)95305-8.

[34] J. Hesse, A. Rübartsch, Model independent evaluation of overlapped Mossbauer spectra, J. Phys. 7 (1974) 526, https://doi.org/10.1088/0022-3735/7/7/012.

[35] B.L. Henke, E.M. Gullikson, J.C. Davis, X-ray interactions: photoabsorption, scattering, transmission, and reflection at E=50-30000 eV, Z=1-92, Atomic Data Nucl. Data Tables 54 (1993) 181, https://doi.org/10.1006/adnd.1993.1013.

[36] C. Jeynes, N.P. Barradas, E. Szilágyi, Accurate determination of quantity of material in thin films by Rutherford backscattering spectrometry, Anal. Chem. 84 (2012) 6061, https://doi.org/10.1021/ac300904c.

[37] A. Błachowski, K. Ruebenbauer, J. Żukrowski, Influence of niobium impurity on spin density in metallic iron, Phys. Status Solidi 242 (2005) 3201, https://doi.org/10.1002/pssb.200541086.

[38] M.T. Raposo, J.D. Ardisson, A.I.C. Persiano, R.A. Mansur, Characterization of phases in the Fe-Nb system, Hyperfine Interact. 83 (1994) 235, https://doi.org/10.1007/BF02074278.

[39] D. Rauch, M. Kraken, F.J. Litterst, S. Süllow, H. Luetkens, M. Brando, T. Forster, J. Sichelschmidt, A. Neubauer, C. Pfleiderer, W.J. Duncan, F.M. Grosche, Spectroscopic study of metallic magnetism in single-crystalline Nb1−yFe2+y, Phys. Rev. B 91 (2015) 174404, https://doi.org/10.1103/PhysRevB.91.174404.

[40] J. Żukrowski, S.M. Dubiel, Mössbauer-effect study of dynamic, magnetic, and electronic properties of C14 Laves phase Nb0.975Fe2.025, J. Appl. Phys. 123 (2018) 223902, https://doi.org/10.1063/1.5023342.

[41] C.L. Chien, K.M. Unruh, Liou, Amorphous FexNb100−x with wide composition range, J. Appl. Phys. 53 (1982) 7756, https://doi.org/10.1063/1.330196.

[42] E. Jartych, D. Oleszak, J.K. Żurawicz, Hyperfine interactions in amorphous Fe–Nb alloys prepared by mechanical alloying, Hyperfine Interact. 136 (2001) 25, https://doi.org/10.1023/A:1015550913839.

[43] K.P. Tai, Y. Dai, B.X. Liu, Metastable phase formation and magnetic properties of the Fe–Nb system studied by atomistic modeling and ion beam mixing, J. Appl. Phys. 104 (2008), 014914, https://doi.org/10.1063/1.2955716.

[44] B. Window, Structural aspects of superlattices of Fe-W, Fe-Mo, and Fe-Nb metals, J. Appl. Phys. 63 (1988) 1080, https://doi.org/10.1063/1.340011.

[45] G.Y. Vélez, G.A. Pérez Alcázar, Ligia E. Zamora, J.A. Tabares, Structural and magnetic study of the Fe2Nb alloy obtained by mechanical alloying and sintering, J. Supercond. Nov. Magnetism 27 (2014) 1279, https://doi.org/10.1007/s10948-013-2428-5.

[46] A.F. Manchón-Gordón, J.J. Ipus, J.S. Blázquez, C.F. Conde, A. Conde, Evolution of Fe environments and phase composition during mechanical amorphization of Fe70Zr30 and Fe70Nb30 alloys, J. Non-Cryst. Solids 494 (2018) 78, https://doi.org/10.1016/j.jnoncrysol.2018.04.061.